Acoustic Detection of Faults and Degradation in a High-Bypass Turbofan Engine During Vehicle Integrated Propulsion Research (VIPR) Phase III Testing

Devin K. Boyle[1]
NASA Armstrong Flight Research Center, Edwards, California, 93523

The Vehicle Integrated Propulsion Research (VIPR) Phase III project was executed at Edwards Air Force Base, California, by the National Aeronautics and Space Administration and several industry, academic, and government partners in the summer of 2015. One of the research objectives was to use external radial acoustic microphone arrays to detect changes in the noise characteristics produced by the research engine during volcanic ash ingestion and seeded fault insertion scenarios involving bleed air valves. Preliminary results indicate the successful acoustic detection of suspected degradation as a result of cumulative exposure to volcanic ash. This detection is shown through progressive changes, particularly in the high-frequency content, as a function of exposure to greater cumulative quantities of ash. Additionally, detection of the simulated failure of the 14th stage stability bleed valve and, to a lesser extent, the station 2.5 stability bleed valve, to their fully-open fail-safe positions was achieved by means of spectral comparisons between nominal (normal valve operation) and seeded fault scenarios.

Nomenclature

AFRC	=	Armstrong Flight Research Center
B&K	=	Brüel & Kjær
CL	=	centerline
EHM	=	engine health management
NASA	=	National Aeronautics and Space Administration
PSD	=	power spectral density
USAF	=	United States Air Force
VAE	=	volcanic ash environment
VIPR	=	Vehicle Integrated Propulsion Research

I. Introduction

THE Vehicle Integrated Propulsion Research Phase III (VIPR III) project was performed during the summer of 2015 at Edwards Air Force Base, California. This project was the third in a series of on-wing tests involving a modified first-generation F117-PW-100 engine (PW2000 military derivative) (Pratt & Whitney, East Hartford, Connecticut) installed on a United States Air Force (USAF) C-17A Globemaster III (The Boeing Company, Chicago, Illinois). The VIPR consisted of four research objectives corresponding four of the major partners, including groups from the National Aeronautics and Space Administration (NASA): [Armstrong Flight Research Center (AFRC) (Edwards, California), Glenn Research Center (Cleveland, Ohio), Langley Research Center (Hampton, Virginia), and Ames Research Center (Moffett Field, California)]; Pratt & Whitney; Boeing Commercial Airplanes (Seattle, Washington); and the USAF Air Force Research Laboratory (AFRL) (Edwards, California). Two of the four objectives are discussed in this paper.

One of the major undertakings of VIPR III was the introduction of volcanic ash into the engine in low concentrations for long durations. The goal of this Volcanic Ash Environment (VAE) research was to simulate the effect of such ash concentrations on the operability and health of a commercially-representative high-bypass turbofan

[1] Aerospace Engineer, Aerodynamics and Propulsion Branch, P.O. Box 273 / MS 2228, AIAA Member.

engine in cruise flight (the engine was operated at a lower power setting than cruise to thermally simulate the cruise conditions in the hot section). The intent of the low concentration exposure was to study the effects in a likely scenario in which the aircraft encounters the distal ash cloud, which in many cases is not visible. For this research, two concentrations were chosen: 1 mg/m^3 and 10 mg/m^3. These concentrations represent the density of volcanic ash suspended in air following a volcanic eruption and subsequent atmospheric dispersion of ash.

The ultimate culmination of the VIPR III testing was to be the accelerated degradation of the F117 test engine potentially to the point at which it would be deemed unserviceable, in order to gain an understanding of engine degradation as a function of volcanic ash exposure. The degradation of the engine to the point of requiring removal from service proved to be a challenge. Nevertheless, the engine did exhibit degradation in the presence of volcanic ash ingestion; this degradation is the basis for the following discussion and indicates a need for further studies.

The primary focus of the NASA Engine Health Management (EHM) research was the use of novel sensors and algorithms under development as well as improvement in awareness of engine health during nominal and seeded fault conditions involving bleed air valves. The station 2.5 and 14th stage stability bleed valves were both operated to their fail-safe (full-open) positions to simulate failure of the valves, which would normally be operated on a schedule dictated by engine conditions. The seeded faults provided an opportunity for a set of acoustic microphones to detect the faults in an ongoing effort to develop a condition-based maintenance technique using simple hardware that is capable of identifying off-nominal engine operation and potentially failed components and their locations. The NASA EHM research built on work completed during VIPR I testing (December 2011) and VIPR II testing (July 2013), during which similar bleed valve faults were introduced.[1]

II. Test Design

During VIPR III, NASA AFRC was the responsible test organization working in conjunction with the Air Force Test Center and research partners. A USAF C-17A aircraft was used with the NASA-owned research engine (F117-PW-100 S/N 170006) installed on the #4 pylon, which is the copilot side outboard engine. The engine had been modified to include several NASA-developed or -sponsored sensors used for Technology Readiness Level advancement of technologies aimed at the improvement of engine health awareness.

The VIPR III testing was performed on a concrete taxiway capable of accommodating the USAF C-17A at full power. Surrounding areas included a mixture of asphalt or concrete, a transition from the pavement to gravel, and finally a desert scrub environment. A representative test setup, showing the aircraft and corresponding hardware orientation, is shown in Fig. 1. It should be noted that this test is far from ideal acoustically. The test area contains many noise sources adjacent to the source (engine)-receiver (microphone) vector. Some extraneous noise sources included air conditioning and ground power carts, compressors, dryers, and the aircraft auxiliary power unit. This analysis intends to analyze trends in the total noise received by the microphones in different locations to suggest an overall degradation in engine condition as a result of volcanic ash ingestion. As such, the relative nature of the signals allows for a more qualitative approach free from the burden of source isolation and elimination. It is assumed that no substantial changes occurred to ancillary equipment during the testing period.

Instrumentation used for data acquisition involved two independent systems for different sets of microphones requiring different recording rates. The first set was a radial array of 11 Brüel & Kjær (B&K) (Naerum, Denmark) Type 4191 ½-inch free-field acoustic microphones oriented at constant 150-ft radii relative to the inlet and core exhaust planes, respectively. The distance corresponds to 60 core exhaust nozzle diameters, which was assumed to be sufficient for far-field conditions to prevail at the microphone. A set of B&K Type 2690 amplifiers provided a 200-V polarization voltage to the microphones, as well as a high-pass filter (20 Hz, to reduce the influence of wind noise). From the amplifiers, the signal was sent to a Ling Dynamic Systems (LDS) Dactron brand Focus II analog to digital recorder, which allowed real-time viewing of the microphone signals on a laptop. The signals were recorded at 65,536 samples/second simultaneously for all channels at a 24-bit resolution. An embedded IRIG-B time code record was included in each channel. Microphone calibrations were performed with a B&K Type 4231 sound calibrator piston-phone providing a 1000 Hz tone at 114 dB. The calibrations were performed at the beginning and end of each test day for each microphone, when there was sufficient time to do so. Otherwise, as many microphones as possible were calibrated before testing began. The multiple daily calibrations were not necessary, however, since there was no appreciable variation in the signal of a given microphone over several days. At any rate, each microphone was compared with its own signal over various days of testing.

Figure 1. Test setup, showing aircraft and microphones F4 and F5 (Photo courtesy: NASA photograph ED15-0188-165).

In addition to the data acquisition system for the far-field microphone array, another system was employed with high-speed recording capability to record data from two B&K Type 4139 ¼-inch free-field acoustic microphones located near the exhaust plane of the test engine. The ¼-inch microphones were calibrated in the same manner as the ½-inch microphones. Figure 2 shows the microphone-aircraft relative locations, including the distances from and orientations with respect to the inlet and exhaust planes. Figure 2 also shows the keep-out zones (cross-hatched regions) for the inlet and jet exhaust. Microphones G1 and G2 were the near-field ¼-inch microphones 25 ft aft and 20 ft sideline on either side of the core exhaust plane (40 ft apart), in order to be as close to the engine as possible without being directly exposed to high-temperature, high-speed exhaust gas. Microphones A1-A6 were positioned aft of the exhaust plane on a constant 150-ft radius, and microphones F1-F5 were located forward of the inlet plane at a constant 150-ft radius. The signal conditioning and data acquisition hardware included B&K Type 2690 amplifiers providing a 200-V polarization voltage and one eight-channel high-rate (2MS/s) Dewetron (Grambach, Austria) data acquisition module simultaneously recording each channel at a rate of 500 kilo-samples/second with a 16-bit resolution. This system also imposed a 20 Hz high-pass filter for reduction of wind noise influences.

Power spectral density (PSD) plots are used to show the changes to the acoustic spectra during VAE and EHM testing. The "pwelch" built-in MATLAB® (The MathWorks, Natick, Massachusetts) function was used, with 75% overlapping rectangular windows.

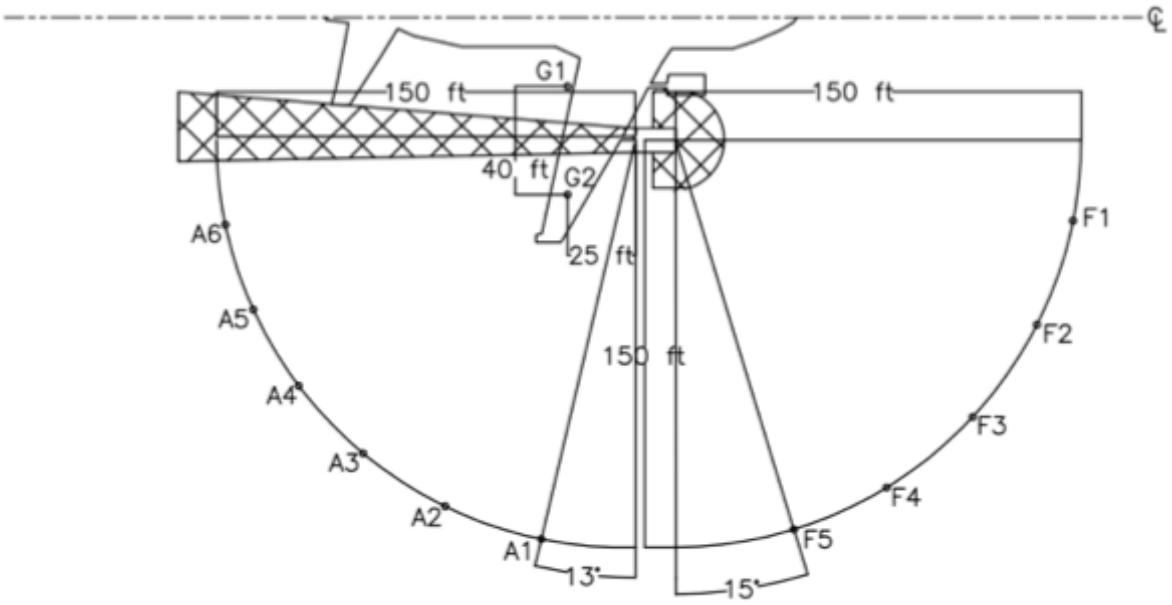

Figure 2. Far-field radial array with microphones F1-F5 and A1-A6 and near-field microphones G1 and G2 positioned behind exhaust plane.

III. Selected Results from Volcanic Ash Environment Testing

One of the most significantly degrading conditions to which the test engine was exposed was the ingestion of volcanic ash in relatively low concentrations for long durations.[2] Figure 3 shows the relationship between exposure duration and concentration of distal ash in the atmosphere. Superimposed on the figure, from left to right, are concentrations/durations that are believed to be economically damaging (not posing danger to the flight, but damaging components irreparably), an unknown region of concentration/exposure duration combination that may be unsafe, followed by a region in which unsafe operation is expected to be certain. The colored ovals correspond to some research flights at low ash concentrations as well as some unintentional encounters that resulted in major engine damage.[3] The VIPR III test points, not shown in the figure, were in the region near the orange dashed line for 1 mg/m^3 for approximately 10 hr and along the black dashed line for 10 mg/m^3 for approximately 10 hr of runtime. The VIPR testing personnel chose these points to bridge either side of the 2 mg/m^3 concentration defined in 2010 by the London Volcanic Ash Advisory Center and provided to European aviation authorities that were expected to be hazardous to flight operations during the 2010 eruption of the Icelandic volcano Eyjafjallajökull. The 2 mg/m^3 threshold is shown in Fig. 3 by the vertical orange dashed line. See Ref. 4 for an example of the ash advisories issued to aircraft; the areas enclosed in red are considered hazardous to aircraft operations.

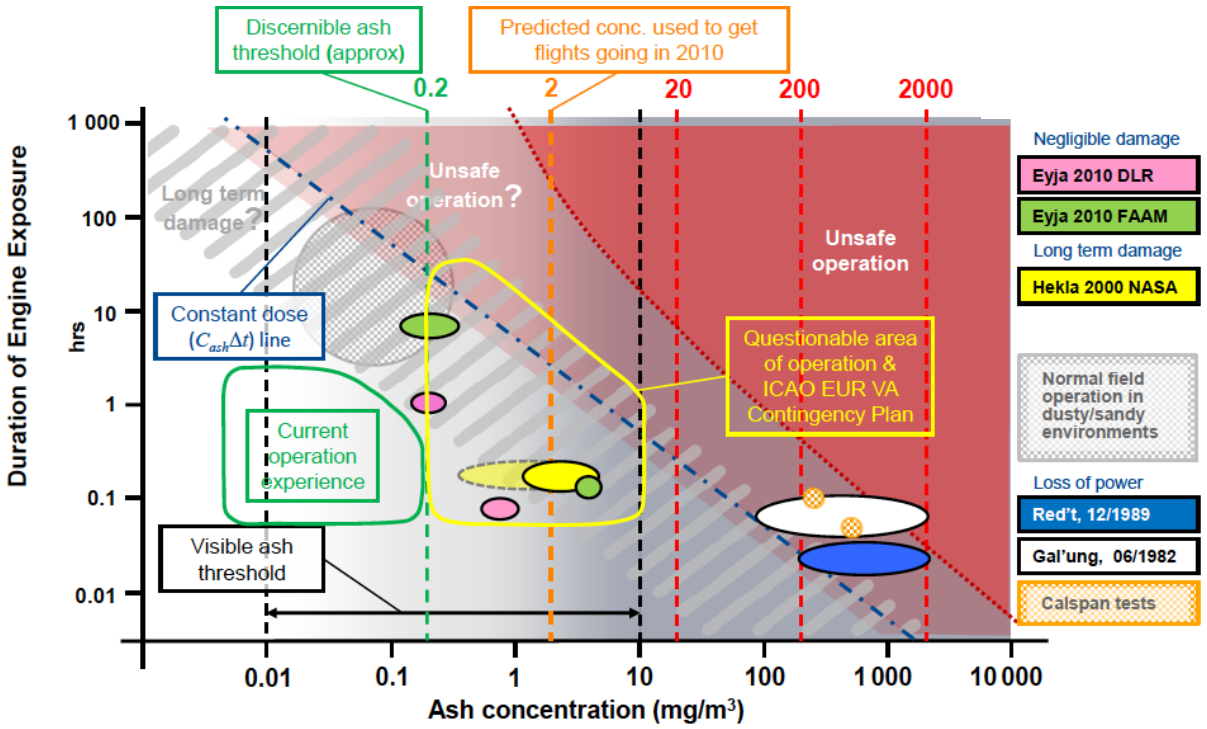

Figure 3. Relationship between volcanic ash concentration and duration as drivers of flight safety and in the context of historical ash encounters. (Used with permission, © 2015 Rolls Royce PLC[2]).

One prominent example of an inadvertent ash encounter occurred when a NASA DC-8 airplane (McDonnell Douglas, now The Boeing Company, Chicago, Illinois) flew through a diffuse volcanic ash cloud from the Mt. Hekla volcano,[5] estimated by the yellow oval on Fig. 3. The engine damage resulting from the encounter necessitated the removal and overhaul of all four engines. In this case, the pilots had no conventional indications of an ash encounter. The only indications came from some very sensitive and specialized instruments which were on board the aircraft for use during the NASA SAGE III Ozone Loss and Validation Experiment (SOLVE) science mission. The images of the DC-8 CFM56 first stage high-pressure turbine blades in Fig. 4 clearly show volcanic ash clogging the turbine cooling passages (left) as well as erosion of the leading edges of the blades (right).

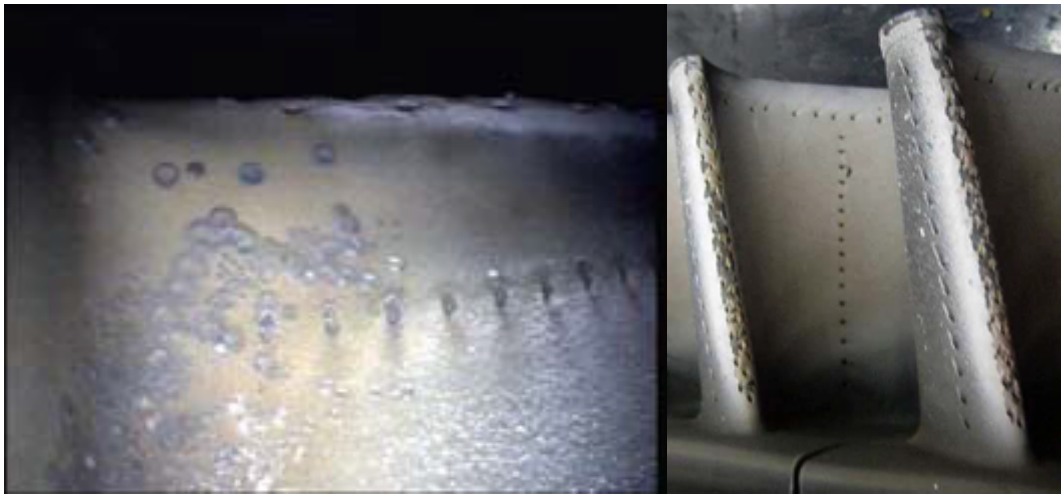

Figure 4. NASA DC-8 CFM56 first stage high-pressure turbine blades showing turbine cooling-hole clogging (left) and leading-edge erosion (right).

The actual "as-run" VIPR III VAE test points included three days of "low concentration" (1 mg/m^3) ash exposure and two days of "high concentration" (10 mg/m^3) for a cumulative mass of approximately 30 kg of volcanic ash into the core of the engine engine. This quantity of ash represented several hours below and above the 2 mg/m^3 threshold defined for safe operations during the 2010 Icelandic eruption. The goal of testing was to render the engine unserviceable at the conclusion, however, the engine proved rather robust and was still operating with a reasonable exhaust gas temperature margin after testing was concluded. For more thorough assessment of the condition of the engine at the conclusion of VIPR III testing, see Ref. 6.

Many of the results present compelling evidence that changes are taking place in the engine as a function of exposure to volcanic ash. In this case the author is suggesting that these changes are a result of cumulative volcanic ash exposure rather than ash concentration. That is not to say that the most pressing failure mechanism in the engine is subject to cumulative exposure rather than total ash concentration or mass density; nevertheless, in this case it is clear that as the engine is exposed to greater cumulative quantities of ash the far-field acoustic changes become evident. The author chose a few more prevalent cases to present in this initial study on the ability of far-field acoustic microphone arrays to detect degradation in the engine.

It must be pointed out that during each day of ash ingestion testing the desert summertime temperatures increased by approximately 11^{o}C from the beginning to the end of testing. Additionally, relative humidities were low and decreased as temperatures increased. Due to the obvious potential for differences in atmospheric absorption of sound to be problematic for this analysis, the author has included the effects of atmospheric attenuation through the use of an attenuation factor. The attenuation coefficient, taken from American National Standards Institute (ANSI) Standard S1.26-1995,[7] was multiplied by the distance of the 150-ft radius used for relative microphone-engine placement and applied to the narrowband sound pressure levels to make comparisons between the ash cycles run at the beginning and end of the test day more relevant. It is clear that the difference in atmospheric attenuation between test points is not nearly enough to explain the difference in spectral power as more ash is introduced to the engine. The figures showing power spectral density as a function of frequency have already been adjusted, removing the effects of atmospheric absorption based on the time period during which each data set was collected.

Since the changes from three days of low concentration testing were unremarkable, the results shown below are exclusively from the high concentration testing. The low concentration testing, however, was performed prior to the high concentration testing, and could have contributed to degradation in the form of imperceptible accumulations and other destructive mechanisms, such as erosion.

Taken from the first day of high concentration testing, Fig. 5 shows the PSD plot for the frequency range between 100-20,000 Hz. The microphone location A5 is the second most aft microphone on the aft arc relative to the exhaust centerline. This microphone exhibited the most prominent difference in level as a function of cumulative duration of ash exposure. From the figure it can be seen that the highest levels, particularly at high frequencies, occur chronologically later in the day, and the level increases as the test progresses, with the highest level occurring at the last ash cycle of the day. An ash ingestion cycle, or "ash cycle," as referenced in the figure, is defined as the period from the start of ash ingestion to the point at which ash flow is stopped to the engine in order to refill the ash hopper. Periodically, events known as shedding of volcanic ash occurred in which visible quantities of ash were exhausted from the engine core in a relatively short period of time. It is unclear yet if those events are individually detectable acoustically and what impact they may have had on reducing degradation. It should be noted that for Fig. 5, two ash cycles are combined for each line shown. Later, each ash cycle is shown individually. The trend continues into the second day of high concentration testing, shown in Fig. 6. The second day of high concentration testing started at a slightly lower spectral level than the first high concentration day. A zoomed section of Fig. 6 is shown in Fig. 7 to more easily discern the changes in spectral level with more ash exposure. Here, each cycle of ash ingestion was captured as a separate signal file, whereas on the previous day each recording contained two cycles. Again, there is a clear increase in spectral power at higher frequencies as a function of more cumulative exposure to volcanic ash. The shift of the tones toward higher frequencies is attributed to the slight increase in rotor speed as temperatures increased throughout the day. The figures present the data from a series of ash ingestion cycles without showing the pre- and post-ash ingestion spectrum. The reason these two periods are omitted from the data is that certain equipment contributing to the overall noise level is not operating at the beginning and end of the test day (it would cause confusion due to the lower level present before ash ingestion). The data presented here show comparable ambient conditions.

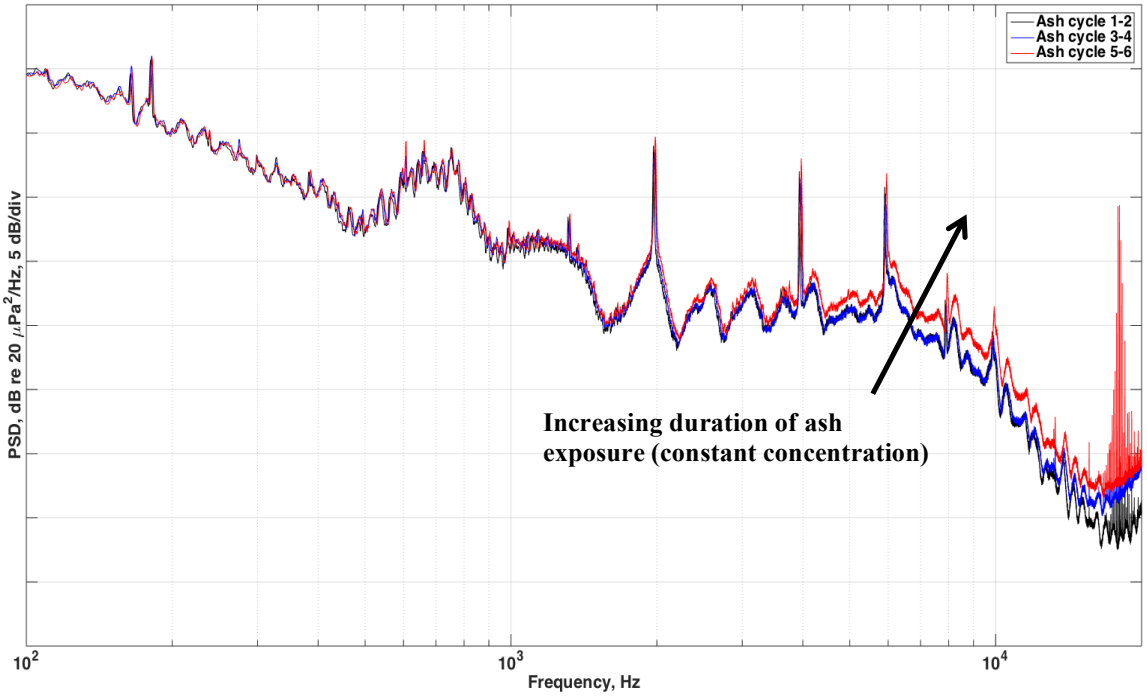

Figure 5. Power spectral density for microphone A5 for several different ash ingestion cycles during the first "high rate" day of VIPR III VAE testing, showing the trend of reducing level as a function of increasing cumulative ash exposure.

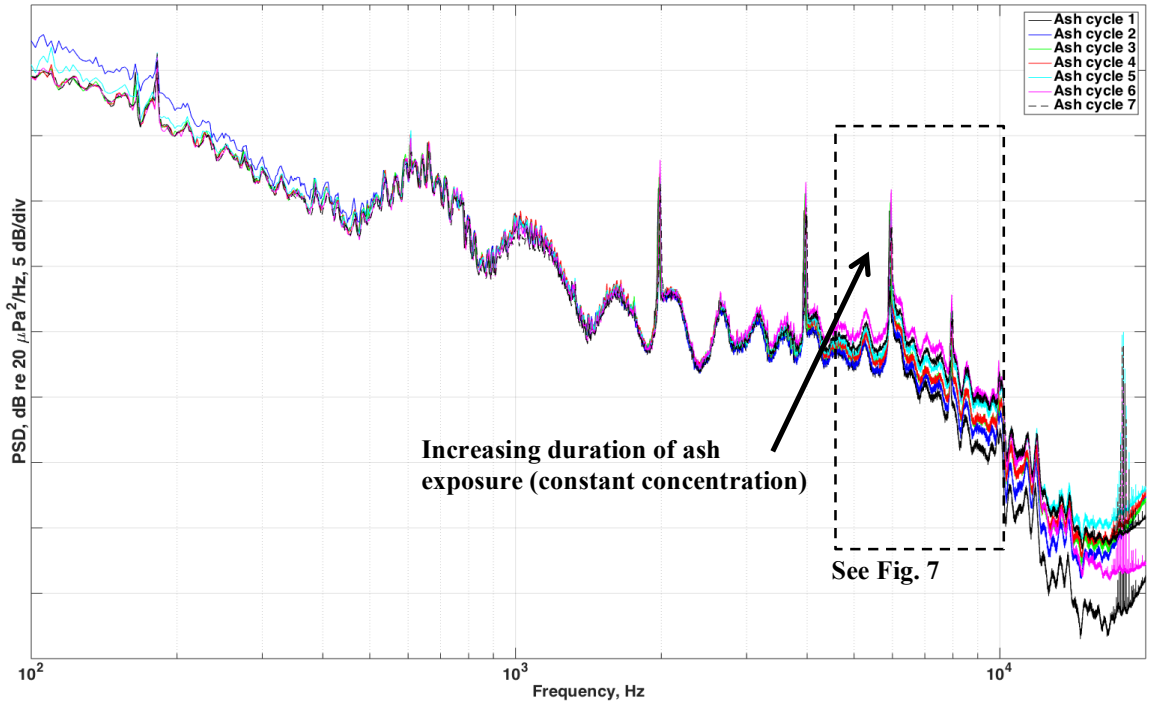

Figure 6. Power spectral density for microphone A5 for several different ash ingestion cycles during the final day of VIPR III VAE testing, showing the trend of reducing level as a function of increasing cumulative ash exposure.

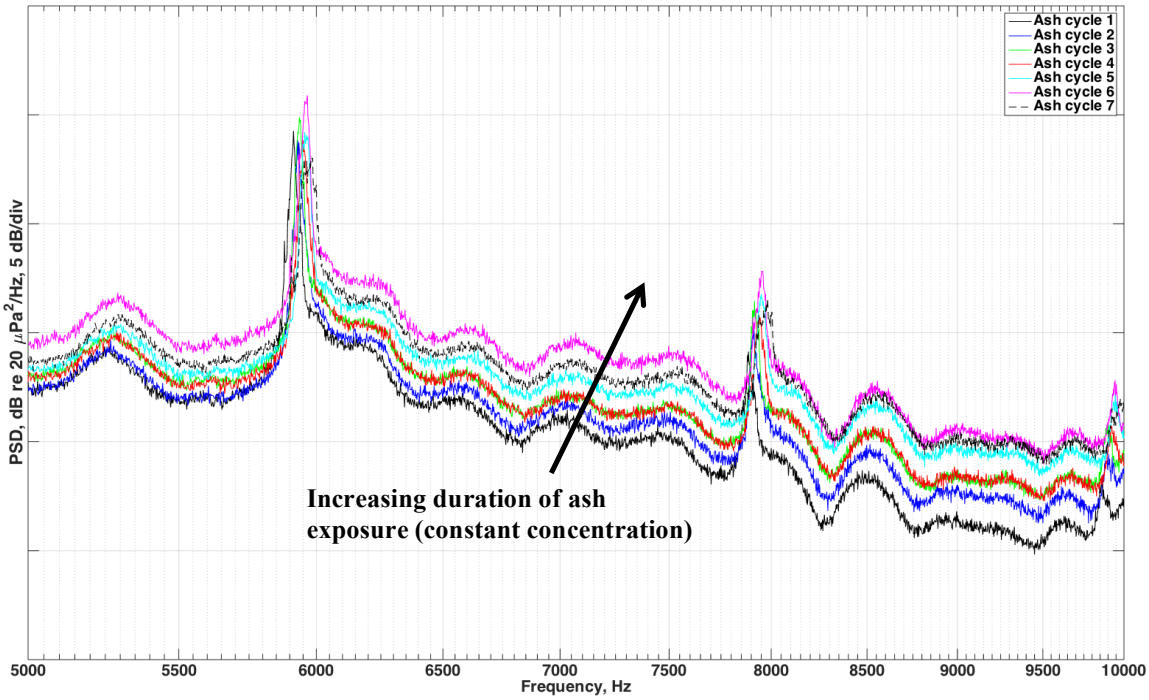

Figure 7. Power spectral density for microphone A5 zoomed in from 5-10kHz, showing the change more clearly as the engine encounters more ash.

Figure 8 demonstrates the same phenomenon at the most aft microphone location A6. Once again, a causal relationship between cumulative volcanic ash ingestion and measurable reduction in spectral power is suggested. The root cause of this change is as yet unclear, but could be from one or several of the degradation mechanisms experienced by turbofan engines in the presence of volcanic ash including: compressor blade erosion, glassification of ash silicates in and around the burner walls and primary combustion zone as well as the first stage turbine vanes and blades, and clogging or erosion of high-pressure turbine cooling passages. This test day included approximately six hours of ash ingestion.

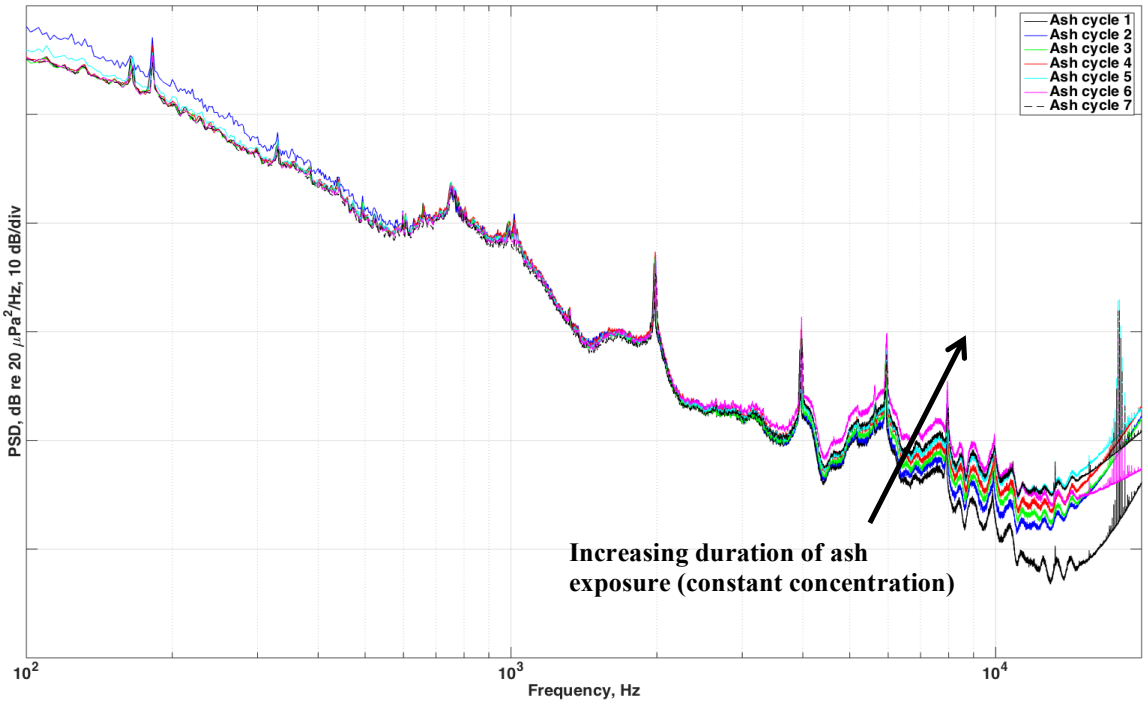

Figure 8. Power spectral density for microphone A6 for several different ash ingestion cycles during the final day of VIPR III VAE testing, showing the trend of reducing level as a function of increasing cumulative ash exposure.

The results obtained here seem to suggest that a relationship exists between the cumulative ingestion of volcanic ash and the progressive degradation of the engine. That relationship may have existed at the 1 mg/m^3 concentration, but may have taken an inordinate amount of time to manifest because of the comparatively small amount of ash ingested relative to the 10 mg/m^3 concentration. This observation brings up an interesting question regarding a single-number metric that could be provided to airlines as a threshold amount above which safety or economic concerns could arise. This possibility was mentioned in Ref. 2 (Clarkson).

IV. Simulated Failure of 14th Stage Bleed Valve

As part of the NASA EHM testing, several stability bleed valves were controlled and forced into off-nominal and fail-safe states during different engine performance phases (static and transient operation). The primary motivation for the use of an acoustic array to detect these faults is a potential application in condition-based maintenance practices wherein the faults could be diagnosed and even localized with these and more sophisticated techniques. These faults were also detected by the far-field microphone array in an effort to further characterize different relevant faults and identify spectral uniqueness for diagnostic purposes. The 14th stage bleed valve, operating only in the fully-open or -closed position, dumps excess bleed air from the high-pressure compressor into the aft bypass duct at a single clock location during start and deceleration to maintain a positive pressure gradient at those conditions. See Fig. 9 for visual details of 14th stage bleed air to the aft bypass duct. The first data sets in Figs. 10 and 11 show aft microphones A4 and A6, respectively, spectral density plots with curves corresponding to noise spectra prior to and after the simulated faulting of the 14th stage bleed valve to its fail-safe fully-open position during a constant power setting. There is a clear and audible broadband noise increase after the valve is opened.

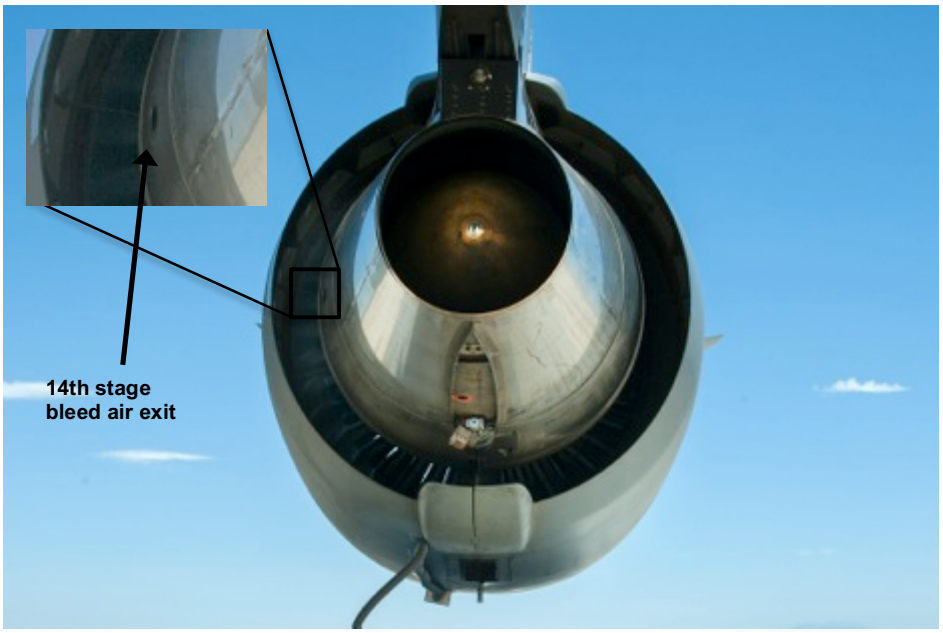

Figure 9. View of test engine looking forward, showing 14th stage bleed air exit into aft bypass duct.

At higher power settings, if the valve fails, it slews open, releasing high-pressure compressor air into the bypass duct, creating a penetrating jet condition with the bypass flow. The noise propagates out the forward and aft bypass duct, as is evidenced by Figs. 10 and 11, and can be seen forward as well in Fig. 12 (microphone location F2, 30 deg relative to inlet centerline axis). Figure 13 shows the aft microphone, A1, at the greatest angle relative to the jet exhaust axis. The change as a result of opening the valve is still plainly evident.

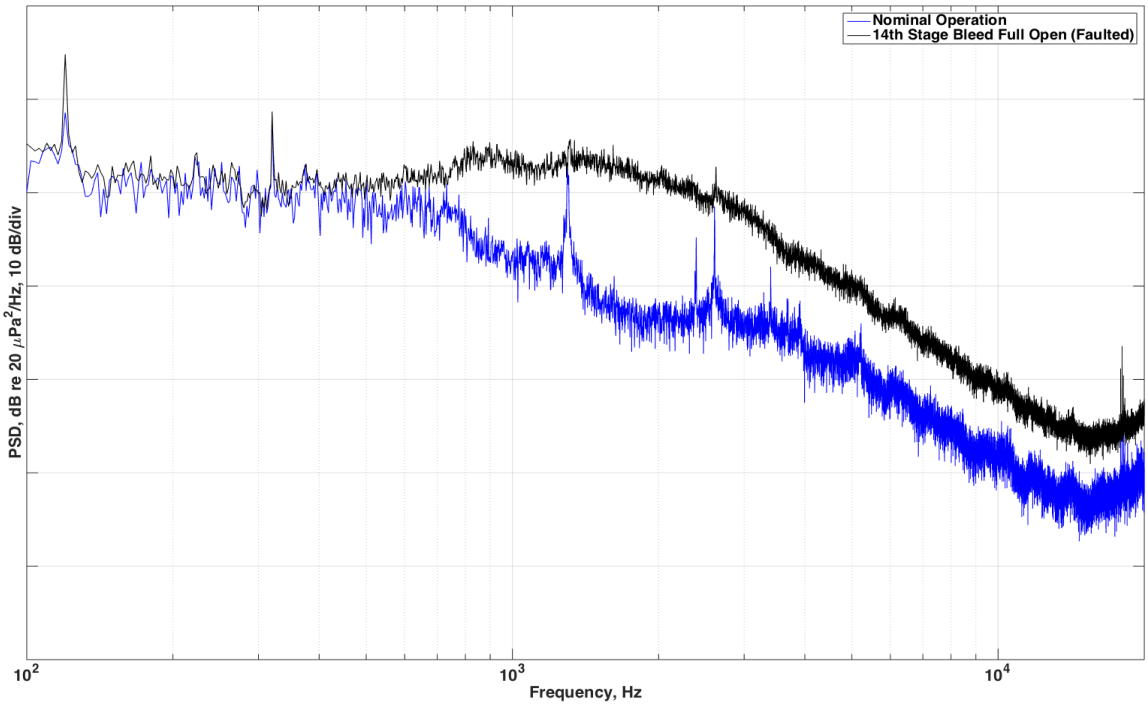

Figure 10. Power spectral density for microphone A4 for simulated failure of the 14th stage bleed valve during steady-state engine operation.

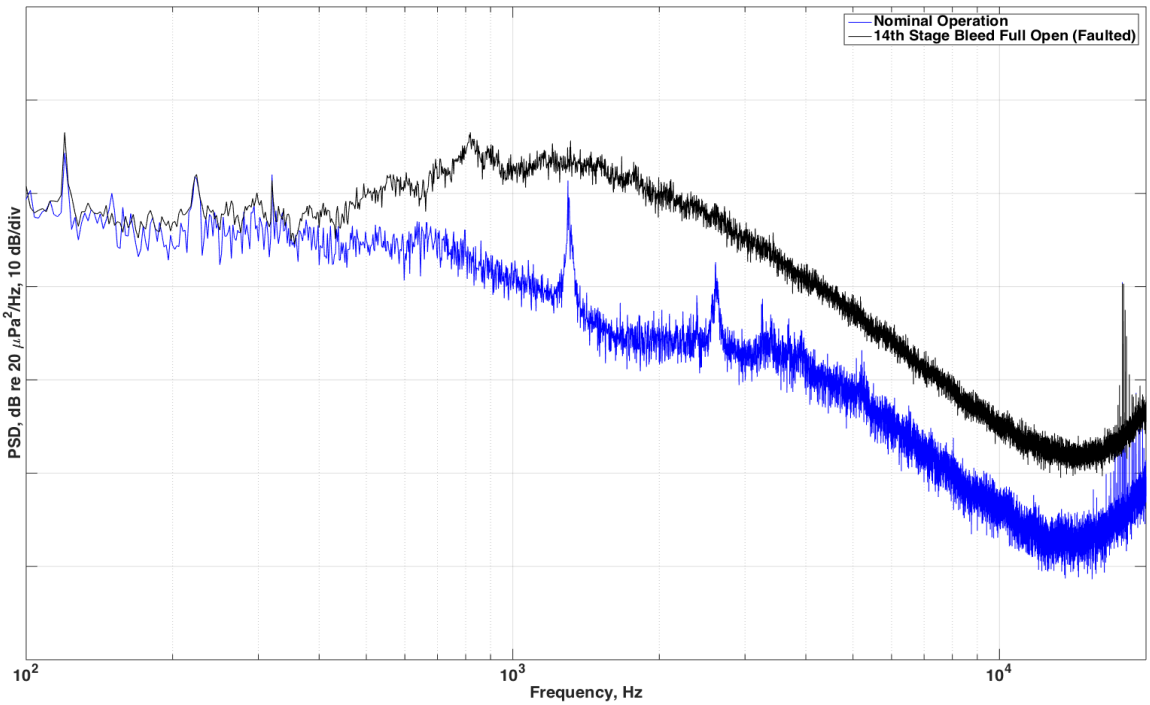

Figure 11. Power spectral density for microphone A6 for simulated failure of the 14th stage bleed valve during steady-state engine operation.

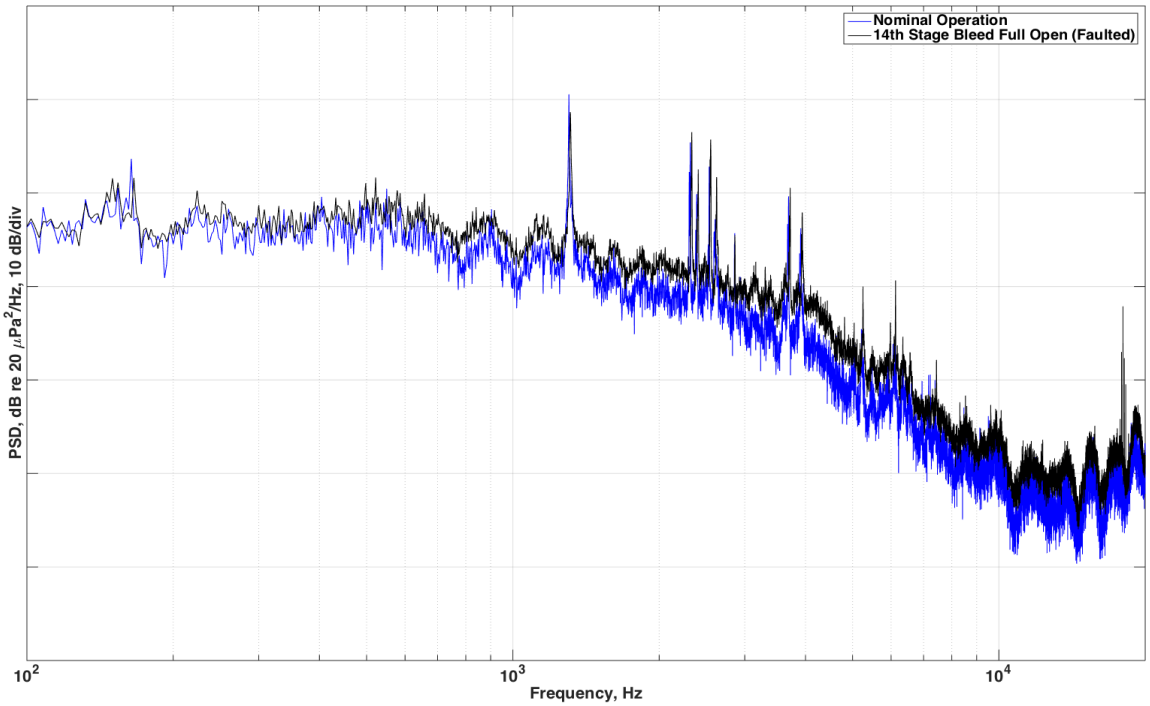

Figure 12. Power spectral density for microphone F2 for simulated failure of the 14th stage bleed valve during steady-state engine operation.

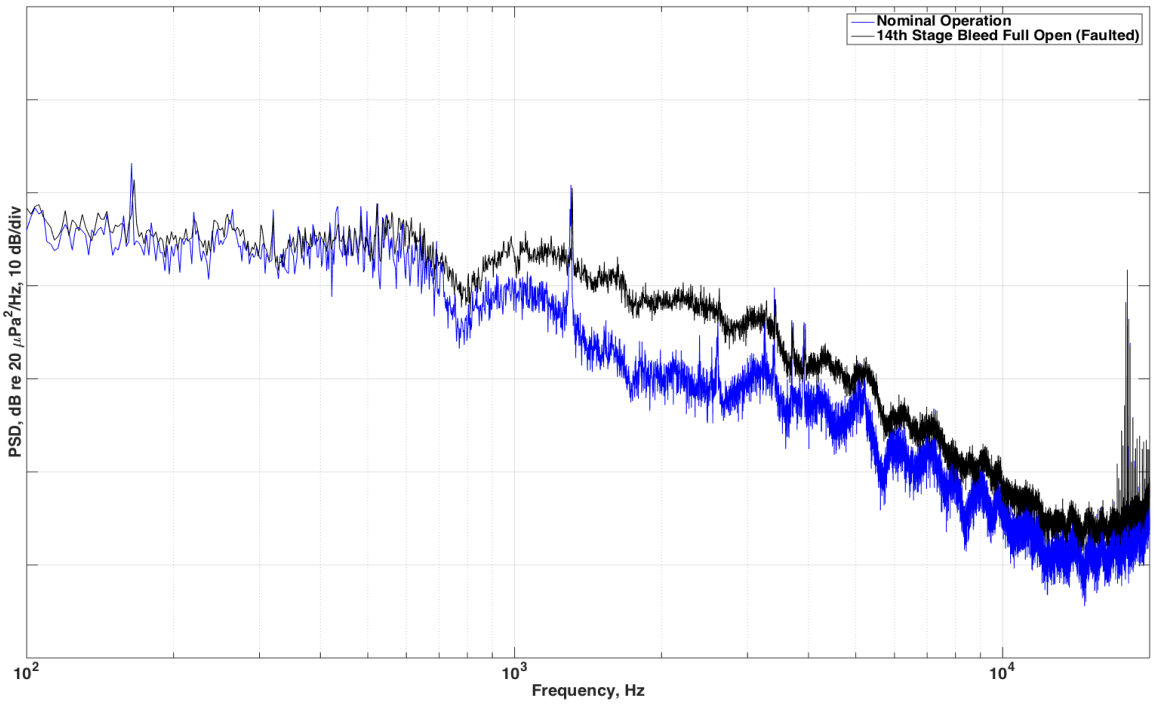

Figure 13. Power spectral density for microphone A1 for simulated failure of the 14th stage bleed valve during steady state engine operation.

Beyond the steady-state operation, simulated valve failures were performed during throttle transients including relatively slow throttle advances and rapid advances of the throttle (referred to here as "ramp" and "snap," respectively). These profiles were performed in two phases: the baseline run with no fault insertion, and the same maneuver with the fault inserted at a particular point, simulating the failure of the valve during a throttle transient. Figures 14 and 15 show the ramp acceleration noise spectra for microphones A4 and A6, respectively. Once again, a broadband increase in the spectra is prominent. The same trend holds true for the case of the snap acceleration profile, the spectra for which are shown for microphones A4 and A6, respectively, in Figs. 16 and 17.

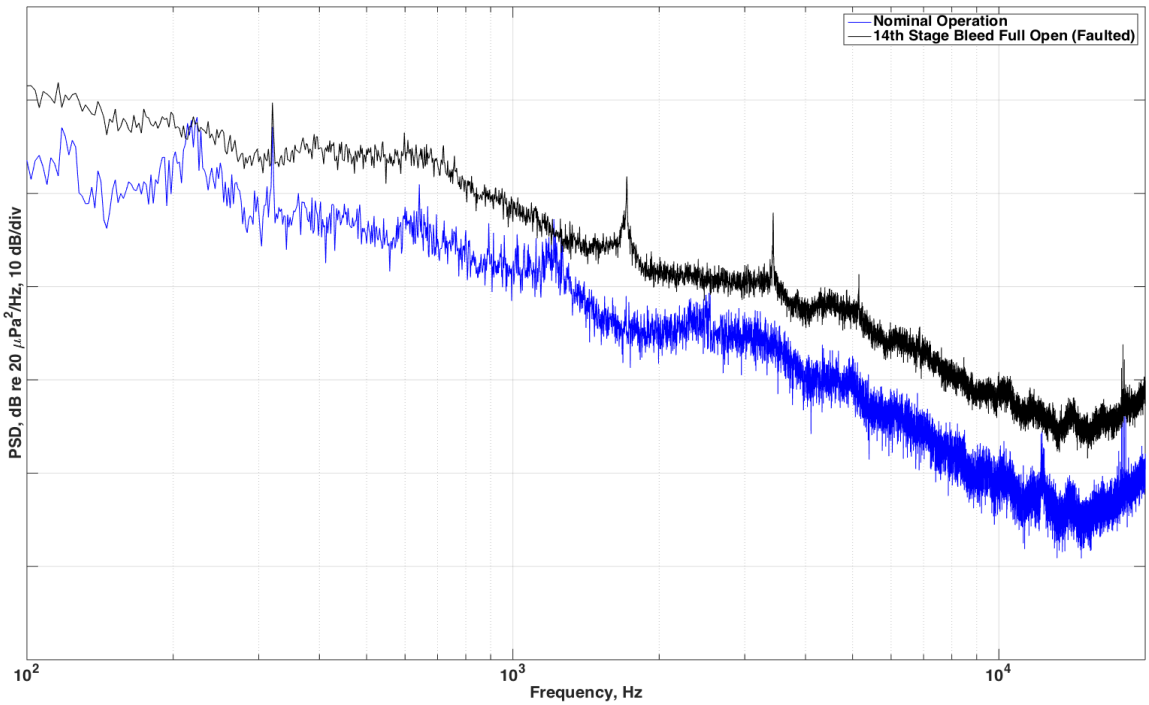

Figure 14. Power spectral density for microphone A4 for simulated failure of the 14th stage bleed valve during ramp acceleration profile.

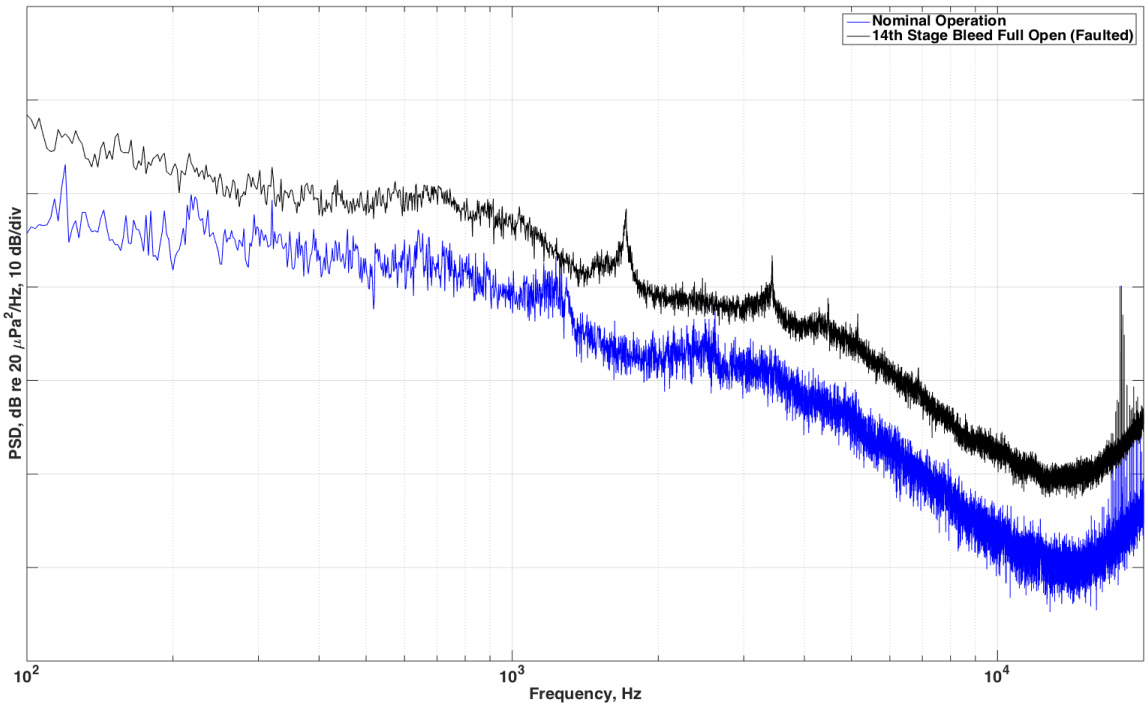

Figure 15. Power spectral density for microphone A6 for simulated failure of the 14th stage bleed valve during ramp acceleration profile.

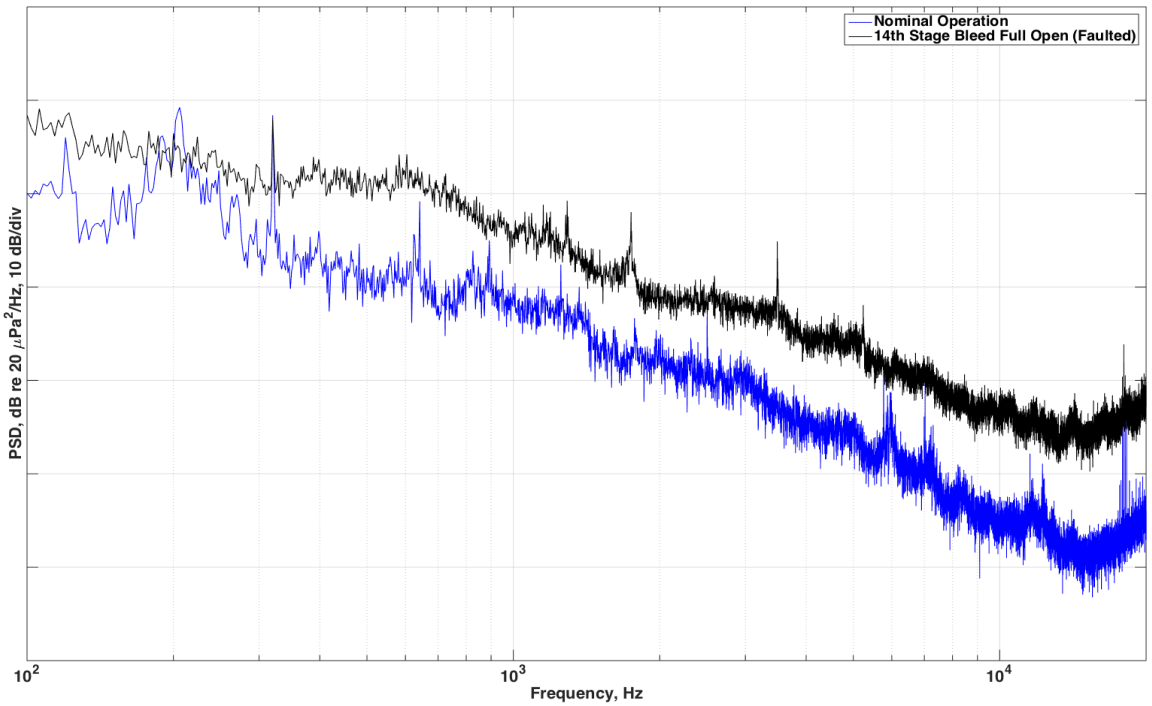

Figure 16. Power spectral density for microphone A4 for simulated failure of the 14th stage bleed valve during snap acceleration profile.

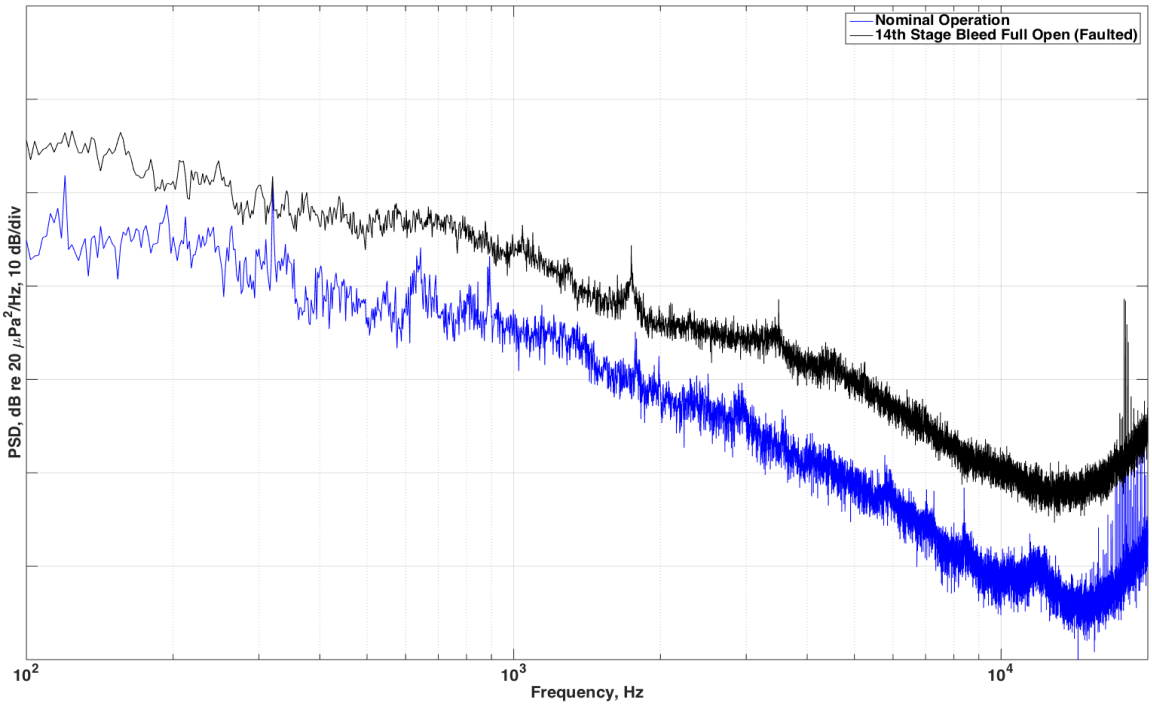

Figure 17. Power spectral density for microphone A6 for simulated failure of the 14th stage bleed valve during snap acceleration profile.

V. Simulated Failure of Station 2.5 Bleed Valve

Simulated failure of the station 2.5 stability bleed valve was conducted during steady-state, ramp, and snap acceleration throttle movements. For several reasons, the detection of the station 2.5 fault was difficult. Firstly, the pressure at station 2.5 (low-pressure compressor exit / high-pressure compressor inlet) is substantially lower than at the 14th stage. Secondly, the valve is modulated from fully open at idle to fully closed before reaching maximum power. As such, the valve is still partially open when it is commanded to its fail-safe fully-open position as opposed to the discretely operating 14th stage valve. Additionally, the station 2.5 bleed valve dumps bleed air at several circumferential locations around the forward bypass duct by way of several rectangular openings in a ring manifold, meaning that the pressure release is distributed around the bypass duct. All of these factors contributed to the relative difficulty of discerning changes in the spectral noise due to the simulated failure of the station 2.5 stability bleed valve. Figure 18 offers some perspective on how the station 2.5 bleed air is dumped into the bypass duct. The difference between the nominal and faulted state was evident for the most forward microphone, F1, seen in Fig. 19.

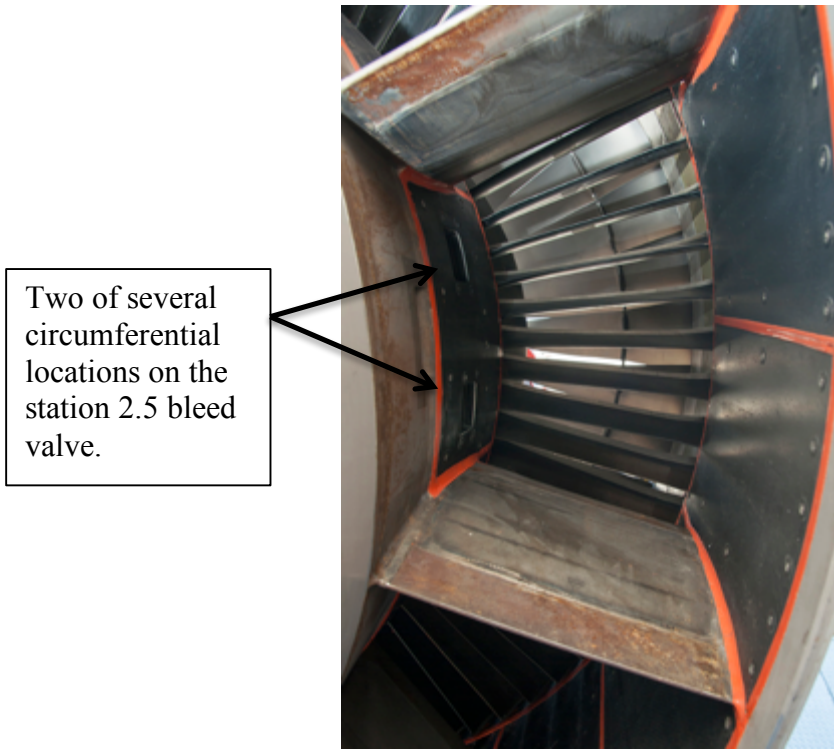

Figure 18. Fan bypass duct looking forward, showing two of several circumferential locations on the station 2.5 bleed manifold.

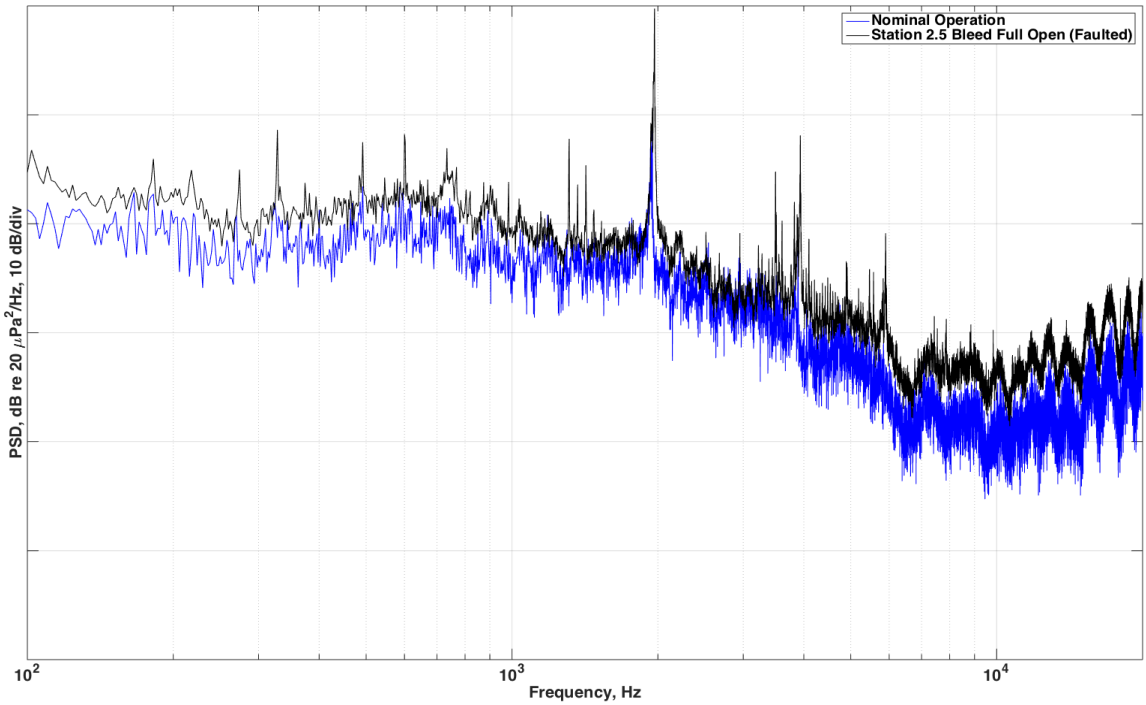

Figure 19. PSD for microphone F1 for simulated failure of the station 2.5 bleed valve during snap acceleration profile.

VI. Conclusion and Future Work

A preliminary study of the use of far-field acoustics to diagnose faults in a commercial aircraft class high-bypass turbofan engine has been presented. The volcanic ash environment testing presented an opportunity to show spectral power changes as a function of ash exposure duration, which suggest that some form of degradation was occurring in the engine as it ingested ash. It will be interesting to see exactly what degradation mechanisms were most prevalent as the engine encountered relatively lower concentrations of volcanic ash for long durations. The results of this testing can provide tremendous insight into the safety and economics of flight operations in slight ash concentrations. This research also might allow operators to install such equipment as will detect off-nominal engine response to volcanic ash or calcium-magnesium-alumina-silicate encounters. Applications may include intermediate or diagnostic maintenance procedures, condition-based maintenance, and non-intrusive, non-destructive inspection cycles.

The National Aeronautics and Space Administration engine health management testing also provided an excellent opportunity to record baseline nominal and seeded fault conditions with respect to stability bleed valve operations. The faults included the manipulation of the bleed valves to the fail-safe and a biased position during static and transient engine operations. Detection of off-nominal conditions was successful during the 14th stage bleed fault testing for both static and transient operations. The station 2.5 bleed valve simulated failure continues to present a challenge to detection, nevertheless, the author continues to work on techniques that may identify the fault of the station 2.5 bleed valve. The data will be used to characterize the spectral shape of the different conditions and try to identify distinctive features of each type of fault in order to develop a diagnostic capability.

Acknowledgments

The author acknowledges the Armstrong Flight Research Center CIF (Center Innovation Fund) for providing funding for the author's CIF research as well as some of the equipment that was used in the Vehicle Integrated Propulsion Research.

References

[1]Boyle, D., "Preliminary Study on Acoustic Detection of Faults Experienced by a High-Bypass Turbofan Engine," AIAA-2014-3106, 2014.

[2]Clarkson, R., "Volcanic Ash and Gas Turbine Aero Engines – Update," https://www.wmo.int/aemp/sites/default/files/RR_Volcanic_Ash_and_Gas_Turbine_Aero_Engines_Update.pdf

[3]Flight Safety Foundation Aviation Safety Network, "ASN Aircraft Accident Boeing 747-236B G-BDXH Jakarta," http://aviation-safety.net/database/record.php?id=19820624-0

[4]Met Office (United Kingdom), http://www.metoffice.gov.uk/aviation/vaac/data/VAG_161750.png

[5]Grindle, T. T., and Burcham, F. W. Jr., "Engine Damage to a NASA DC-8-72 Airplane From a High-Altitude Encounter With a Diffuse Volcanic Ash Cloud," NASA/TM-2003-212030, 2003.

[6] Venti, M., Lekki, J., and Loykraft, G., "Vehicle Integrated Propulsion Research (VIPR) III Volcanic Ash Environment (VAE) Preliminary Visual and Teardown Observations," https://ntrs.nasa.gov/archive/nasa/casi.ntrs.nasa.gov/20160003579.pdf [cited December 1, 2016].

[7]American National Standards Institute, Inc., *Method for Calculation of the Absorption of Sound by the Atmosphere*, ANSI S1.26-1995, 1995.